JACS
JOURNAL OF THE AMERICAN CHEMICAL SOCIETY

ARTICLE

pubs.acs.org/JACS

Toward Complementary Ionic Circuits: The *npn* Ion Bipolar Junction Transistor

Klas Tybrandt, Erik O. Gabrielsson, and Magnus Berggren*

Department of Science and Technology, Organic Electronics, Linköping University, SE-601 74 Norrköping, Sweden

Supporting Information

ABSTRACT: Many biomolecules are charged and may therefore be transported with ionic currents. As a step toward addressable ionic delivery circuits, we report on the development of a *npn* ion bipolar junction transistor (*npn*-IBJT) as an active control element of anionic currents in general, and specifically, demonstrate actively modulated delivery of the neurotransmitter glutamic acid. The functional materials of this transistor are ion exchange layers and conjugated polymers. The *npn*-IBJT shows stable transistor characteristics over extensive time of operation and ion current switch times below 10 s. Our results promise complementary chemical circuits similar to the electronic equivalence, which has proven invaluable in conventional electronic applications.

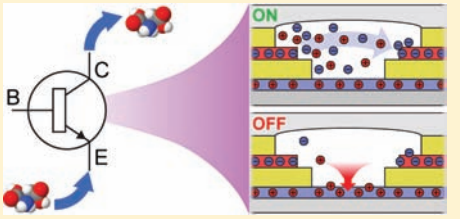

INTRODUCTION

Electrophoretic delivery of ions and charged biomolecules is attractive since it induces little convection, it does not rely on moving mechanical parts, and the delivered amount of substance can be correlated to the electric current.[1,2] Delivery rate and temporal control can be mediated through the applied voltage. However, to achieve more advanced features, such as addressability in a delivery matrix circuit, active components that exhibit nonlinear device characteristics are needed. In conventional electronics these components are often diodes and transistors.[3] Diodes are two terminal devices with the property of current rectification while transistors generally are three terminal devices in which the current between two terminals can be modulated and amplified by a third terminal. To mimic electronic circuits and construct ionic circuits, in which ions and charged biomolecules are transported, ionic transistors and diodes must be developed. Ideally, these ionic transistors should have a high ratio between the on and off current to minimize leakage, a fast switching speed, and a high current gain. Further, they should be functional at physiological conditions and be possible to integrate into a larger system. Recently, nanofluidic transistors and diodes have received a lot of attention.[4−6] In these devices the surface charge along the walls of the thin channels modulates the conductivity through the device. Although these devices show diode- and transistor-like behavior, they are typically only functional at relatively low salt concentrations as the Debye screening length at 100 mM is ∼1 nm. Other routes for constructing ionic transistors have been explored but without successful operation at physiological conditions.[7]

An alternative approach to achieve ionic transistors is to utilize ion exchange membranes.[8] These membranes contain fixed ionic groups which are compensated for by mobile ions of the opposite charge (counterions). The electrostatic repulsion (Donnan exclusion) of mobile ions of the same charge (co-ions) as the fixed groups renders the membrane selective to the counterions, even at physiological conditions.[8] Cation- and anion-selective membranes are in many aspects the ionic equivalent to *p*- and *n*-doped semiconductors, respectively. By sandwiching a cation- and an anion-selective membrane a bipolar membrane (BM) is obtained.[9,10] BMs exhibit current rectification in similarity to bipolar semiconductor *pn*-junction diodes. The rectification is caused by depletion and enrichment of mobile ions between the membranes at reverse and forward bias, respectively. BMs are used in a variety of applications,[11] e.g., in electrodialytic water splitting, and more recently as diodes in ionic circuits.[12] However, logic circuits entirely composed of diodes are passive and exhibit severe limitations, such as lack of gain, inability to realize all logic functions, and eroding signal values. Therefore diode logic is typically only used for simple operations of low complexity. Also ionic diodes may suffer from hysteresis, as in the forward bias salt ions accumulate within the junction and eventually cross over to the previously excluded side,[10] thus leaving the system in a changed state.

To go beyond the limitations of diode-based ionic circuits, we recently reported an ion bipolar junction transistor (IBJT).[13] This ionic transistor was of the *pnp*-type and can modulate the transport of cations at physiological conditions. Here we report on the development of the complementary version of this device, the *npn*-IBJT (Figure 1). The characteristics of the device are presented along with a demonstration of modulated transport of the biologically relevant neurotransmitter glutamic acid. Not only does this device allow for regulation of anionic currents, but in combination with the *pnp*-IBJT it also enables construction of complementary circuits, which has proven very fruitful in the conventional electronics industry.[14]

RESULTS AND DISCUSSION

Device Architecture and Operation. The *npn*-IBJT consists of anion-selective emitter and collector, cation-selective base, and

Received: January 28, 2011
Published: May 20, 2011

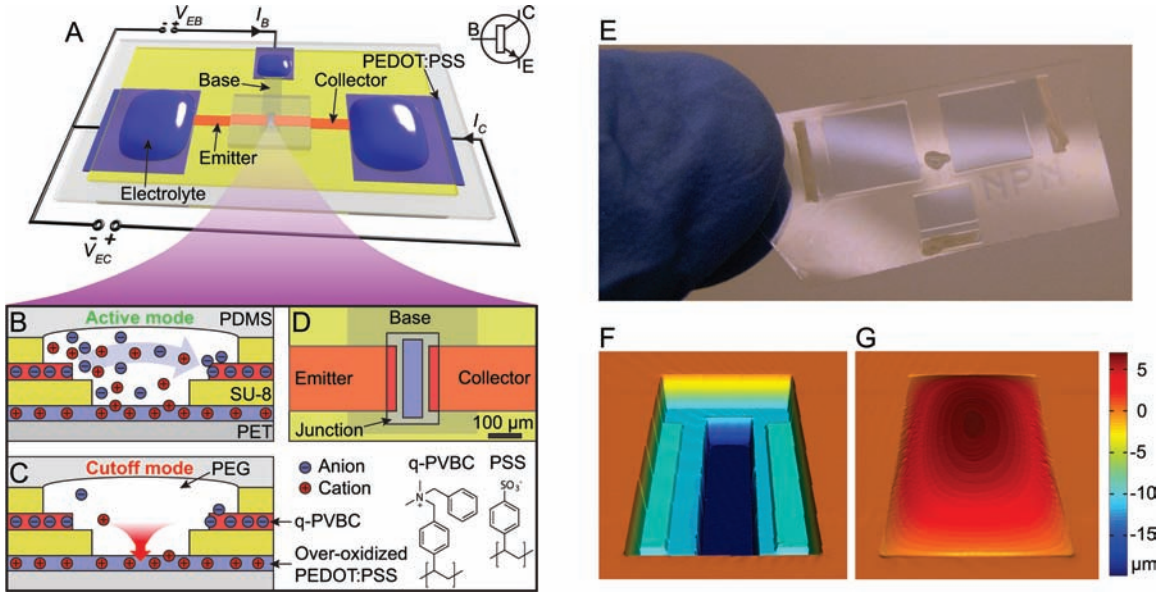

Figure 1. *npn*-IBJT. (A) The emitter and collector are separated from the base by a neutral polymer electrolyte. Conductive PEDOT:PSS electrodes covered by electrolytes inject/extract ions to/from the terminals of the transistor. (B) In the active mode the base supplies the junction with cations. (C) In the cutoff mode the base depletes the junction of mobile cations. (D) The junction is formed by an opening in the SU-8 insulation layers which is filled with a polymer electrolyte. The distance between the emitter and collector is 100 μm. (E) Photograph of the fabricated device with painted silver contacts. The three PEDOT:PSS electrodes and the PDMS encapsulation are visible. (F) Measured topographies of the junction before and (G) after the PEG electrolyte was applied.

a neutral polymer electrolyte junction (Figure 1). The device can be seen as two BM diodes (emitter−base (E−B) and collector−base (C−B)) which share the same base and junction (J). A thin film of the conductive polymer[15,16] poly(3,4-ethylenedioxythiophene)[17] doped with the polyanion poly(styrenesulfonate) (PEDOT:PSS) coated on a plastic (PET) foil is used as substrate. The cation-selective base comprises overoxidized[18] PEDOT:PSS, i.e., leaving PSS ionically conductive and PEDOT electronically nonconducting. Two 10 μm thick insulating layers of SU-8 are deposited on top of the PEDOT:PSS pattern with openings located at the electrodes and at the junction (Figure 1D). The emitter and collector are patterned between the two SU-8 layers and are in contact with the neutral poly(ethylene glycol) (PEG) electrolyte (Figures 1B−D). The anion-selective layer is ∼700 nm thick and consists of poly(vinylbenzyl chloride) partly quaternized by *N*-benzyldimethylamine (labeled q-PVBC, Figure 1) and cross-linked with 1,4-diazabicyclo[2.2.2]octane. The junction is covered by a poly(dimethylsiloxane) (PDMS) layer to encapsulate the polymer electrolyte. The fabricated structure was verified with optical profilometry before and after the PEG gel was applied (Figure 1F,G). A photograph of the complete device is shown in Figure 1E.

Electric currents are translated into ionic ones at the patterned PEDOT:PSS electrodes,[19] which in part are covered by aqueous electrolytes, according to the electrochemical reaction $PEDOT^+:PSS^- + M^+(aq) + e^- \leftrightarrow PEDOT^0 + M^+:PSS^-$. The counterions in the ion exchange membranes need absorbed water to dissociate and become mobile; thus, it is necessary to soak the devices in water prior to use. The common-emitter transistor configuration (Figure 1A) was used throughout this work. When the electric potential at the base is lower than the potential at the emitter and collector ($V_{EB} < \sim 0$) the transistor is in cutoff mode (Figure 1C). In this mode the base depletes the junction of cations, thus lowering the ion concentration in the bulk of the junction (c_J) which results in a low collector current (I_C) (Figure 2A). In the

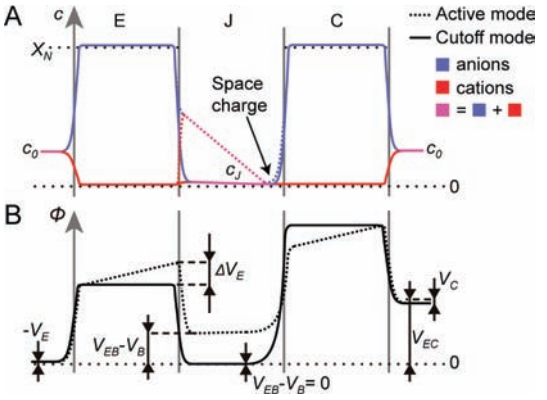

Figure 2. Schematic drawings of concentrations and electric potentials. (A) The concentration of fix charges (X_N) is much higher than the electrolyte concentration (c_0), thereby excluding cations from the membrane. In the active mode a linear diffusion gradient is created inside the junction. (B) In the cutoff mode the whole potential drop occurs at the junction−collector interface. In the active mode there are resistive potential drops (ΔV_E) inside the emitter and collector. The potential drops over the electrodes (V_E, V_C, and V_B) are small compared to V_{EC}.

cutoff mode both the E−B and the C−B diodes are reversely biased. When increasing the potential of the base so only the E−B diode is in forward bias ($\sim 0 < V_{EB} < \sim V_{EC}/2$), the transistor operates in the active mode (Figure 1B). Cations are injected from the base and compensated for by anions, primarily from the emitter, thus increasing c_J and correspondingly I_C. The resistive potential drop over the emitter (ΔV_E, Figure 2B) increases along with I_C and causes the potential drop across the E−B junction to decrease until the base current (I_B) equals the E−B leakage current, i.e., steady state. Because I_B is small at steady state and ΔV_E approximately equals V_{EB}, I_C is expected to depend linearly

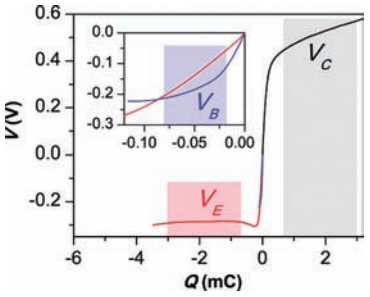

Figure 3. Potential drops over the electrodes as a function of transported charge. The colored regions indicate the range of transported charge in which the characterization was performed. The currents for V_C, V_E, and V_B were +300, −300, and −20 nA, respectively.

on V_{EB}: $I_C = R_E(V_{EB} - V_T)$, where V_T is the threshold voltage. The threshold voltage may include contributions from potential drops over the electrodes, in the junction, and so on, but its explicit dependences are not clear at this stage.

Insights into the active mode transport processes occurring inside the junction can be gained from the theory of overlimiting currents for ion exchange membranes.[20] According to this theory a linear diffusion gradient is created from the emitter to the collector within the bulk of the junction with I_C proportional to Δc_J (Figure 2A). At the J−C interface an extended space charge layer is formed with a high electric field which accounts for most of the potential drop within the junction.[20,21] In the cutoff mode, I_C is negligible and the entire potential drop occurs at the J−C interface. When $V_{EB} > \sim V_{EC}/2$, both diodes are in forward bias and the transistor operates in the so-called saturation mode. In this mode I_B is high and causes ion accumulation within the junction, resulting in failure of membrane selectivity due to the high salt concentration.

Device Characteristics. Characterization was performed with aqueous 0.1 M NaCl electrolytes at all electrodes. The potential drops over the electrodes were measured by having all three electrodes in contact with a common electrolyte and source a current between two of them while using the third as reference. The potential drop can be divided into two contributions, one from the shift in redox state of the PEDOT and one from the overpotential necessary to drive a current through the electrode. Thus, to get an upper boundary of the potential drops over the emitter and collector electrodes, a current of 300 nA ($>I_{C,max}$) was sourced between the two electrodes. Since I_B was slightly negative on average during the characterization, a current of −20 nA was used to measure the potential drop over the base electrode. The colored regions in Figure 3 show the range of charging for which the characterization data below were obtained. When switching off the current, the electrode potentials decrease and after 1 h quite stable values are reached, which constitute a lower limit for the potential drops during characterization (Figure S1A of the Supporting Information). Thus one expects $0.3 < V_C < 0.6$ V, $0.1 < -V_E < 0.3$ V, and $0.1 < -V_B < 0.3$ V. The short-term shifts in base electrode potential when charging with relevant amounts ($<3\,\mu$C) were found to be small (Figure S1B).

A prerequisite for good IBJT functionality is that the diodes work properly. Therefore, the E−B diode was characterized separately by disconnecting V_{EC} and cycling V_{EB} from −6 to +3 V (Figure 4A). In the forward bias the conductivity of the junction is high and the resistive loads of the emitter and base channels dominate the behavior, which results in a linear slope. When entering into reverse bias, the salt is extracted out of the junction by a negative current. As the junction becomes depleted of mobile ions, its resistance increases and I_C drops. Over a complete cycle, the amount of extracted charge differs less than 2% from the amount of injected charge; i.e., the leakage out from the junction is low. The measured current rectification ratio $|I_B(+3\,V)/I_B(-3\,V)|$ was 35, comparable to previously reported rectification ratios for BMs.[22] After depletion of the junction I_B remains low in the reverse bias, indicating that no pronounced field-enhanced water dissociation occurs.

The transistor response when switching between active and cutoff mode is of great interest. These current transients were measured by applying a voltage pulse to V_{EB} from −3 to +3 V while keeping V_{EC} = 10 V (Figure 4B). When switched on, I_B is initially high but stabilizes quickly as I_C rises and reaches steady state. When V_{EB} is turned off, I_B depletes the junction of mobile cations, causing a fast decrease in I_C. The 90% rise time of I_C is 9 s and the 10% fall time is 3 s. The on−off ratio of the shown component was 30; however, on−off ratios above 100 have been achieved for other components. Static transistor characteristics are useful for incorporating transistors into circuits. The transfer curve was obtained by scanning V_{EB} back and forth between −2 and +3 V (2.5 mV/s) while keeping V_{EC} = 10 V (Figure 4C). As predicted I_C increases linearly versus V_{EB} in the active mode and is low in the cutoff mode ($V_{EB} < V_T = -0.2$ V). Advantageously, only minor hysteresis was present and I_B remained low throughout the whole scan. Furthermore, the current−voltage output characteristics were obtained for different fixed values of V_{EB} by ramping V_{EC} (3 mV/s) in the active mode (Figure 4D). I_C is predicted to show saturation behavior with respect to V_{EC}, which also was measured in our devices. The saturation mode was avoided in these measurements due to the high I_B and c_J in this mode, which have been found to have a negative impact on device stability. If it is desirable to run the device in saturation mode in the future, the problem with high I_B might be solved by increasing the resistive load of the base significantly. Finally the *npn*-IBJT was characterized with floating base (Figure 4E). While in the cutoff mode, the base was disconnected and it was found that larger V_{EC} gave faster increase in and higher I_C. When 10 mM NaOH was mixed into the 0.1 M NaCl emitter electrolyte, I_C reached a significantly lower value. The floating base current can be attributed to a buildup of c_J due to a small amount of water dissociation in the space charge layer at the collector interface. When hydroxide ions are transported from the emitter into the junction, the proton concentration decreases together with I_C.

All of the transistor characterization data above is from one device for consistency reasons; however, several substrates with devices have been fabricated and tested. The largest variations in yield and performance were found to be between different substrates, probably caused by fabrication issues. Within a successfully processed substrate, the resistivities of the channels were similar and the parameter which typically distinguished good from poor devices was the off current level, which could differ by as much as a factor of 10. The devices had to be switched on and off 5−20 times in order to achieve stable performance, likely due to initial changes in the ionic transport properties of the channels and the junction. After initialization, steady-state levels of I_C drifted about 15% over 5 h of operation.

Modulation of Glutamic Acid Delivery. We have recently shown that organic conducting materials can be used in vitro and in vivo to translate electric signals into precise delivery of positively charged chemical messengers.[2,23,24] To evaluate if the present *npn*-IBJT can be used in a corresponding manner, i.e., as an addressable delivery point for negatively charged

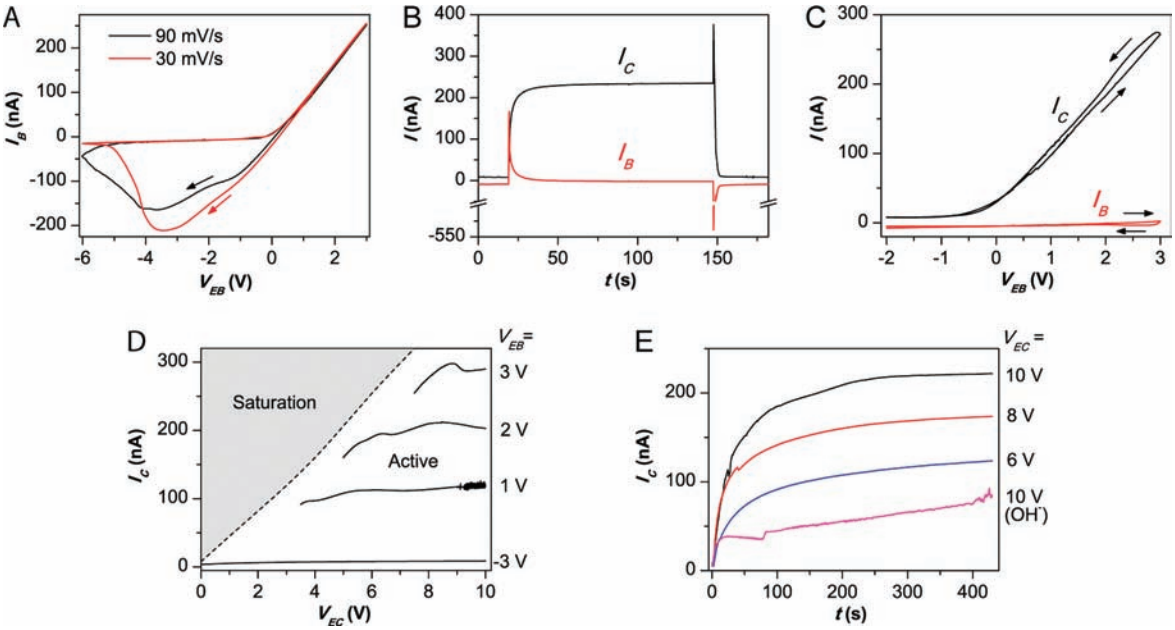

Figure 4. Diode and transistor characteristics. (A) The emitter−base diode has a linear slope in the forward bias due to the resistive load of the emitter and base channels. In the reverse bias salt is initially extracted from the junction, eventually leading to depletion with a higher resistance and a lower current. (B) The switching transients for a voltage pulse in V_{EB} from −3 to +3 V. The 90% rise and 10% fall times are 9 and 3 s, respectively. (C) The transfer curve (I_C) is linear for higher V_{EB} and has little hysteresis. I_B remains low during the entire scan. (D) The output characteristics reveal saturation behavior in the active mode. The saturation mode was avoided due to high base currents. (E) The panel shows I_C upon switching from the cutoff mode to floating base. A basic emitter electrolyte limits I_C are due to recombination of protons and hydroxide ions inside the junction.

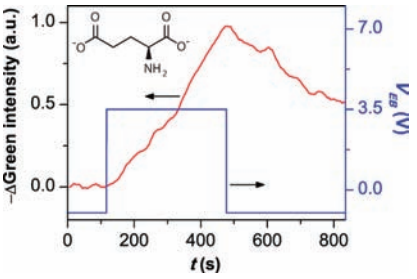

Figure 5. Actively modulated Glu transport. The emitter electrolyte comprises 0.05 M Glu and 0.05 M NaCl while the collector electrolyte contains a colorimetric detection kit for Glu. In the cutoff mode no color change is observed 40 μm from the outlet. When switched on, the Glu induced color change increases until the device is turned off. Upon delivery stoppage the Glu and dye concentration at the outlet starts to decrease due to diffusion.

biomolecules, the transport of the neurotransmitter glutamic acid (Glu) was studied. The emitter electrolyte comprised 0.05 M Glu and 0.05 M NaCl whereas the collector electrolyte was loaded with a colorimetric detection kit for Glu. The color change at 40 μm from the outlet was recorded with a microscope and analyzed (Figure S2 of the Supporting Information). The normalized extracted color change in the green channel can be seen in Figure 5 as the *npn*-IBJT is switched on and off by changing V_{EB}. Immediately after switching on, the Glu delivery starts and the corresponding color change is visible. After turning off the *npn*-IBJT, the actual delivery stops and the released Glu molecules as well as the activated dye diffuse away, resulting in a decrease in absorption. This shows that the *npn*-IBJT is feasible for controlling transport of both inorganic anions as well as smaller negatively charged biomolecules.

CONCLUSION

With this work, we have demonstrated how *npn*-IBJTs can be constructed utilizing standard microfabrication techniques. Currently, the transistor characteristics of our *npn*-IBJTs including high on−off ratios, stable current levels, and dynamic modulation outperform other kinds of ionic transistors running at physiological conditions. The design is prepared for integration of both *npn*- and *pnp*-IBJTs manufactured on the same chip without additional fabrication steps. Since the *n*- and *p*-channels are vertically separated from each other, they can cross without the need of additional insulation and vertical interconnects. Furthermore, the improved design allows for un-cross-linked polymer electrolytes to be used in the junction, offering greater flexibility with respect to materials in general and thereby opening up for future performance improvements. Altogether, our findings lay the groundwork for realization of complementary ionic circuits, e.g., addressable delivery systems for charged biomolecules. We envisage that such ionic circuits will have impact in various fields including sensors,[25] lab-on-a-chip,[26] drug delivery,[27] and electrochemical components.[28]

ASSOCIATED CONTENT

Supporting Information. Text describing experimental details and figures showing transient electrode potential measurements and microscope images of Glu detection. This material is available free of charge via the Internet at http://pubs.acs.org.

AUTHOR INFORMATION

Corresponding Author
magbe@itn.liu.se

■ ACKNOWLEDGMENT

The research was financed by the Swedish Foundation for Strategic Research (OBOE—Strategic Research Center for Organic Bioelectronics), the Knut and Alice Wallenberg Foundation, the Royal Swedish Academy of Science, the Swedish Research Council (Grant 621-2008-2642), and the Önnesjö Foundation. We also acknowledge Professor Robert Forchheimer and Dr. Edwin Jager, both at Linköping University, as well as Dr. Mats Sandberg and Dr. David Nilsson at Acreo AB, for fruitful discussions.

■ REFERENCES

(1) Kalia, Y. N.; Naik, A.; Garrison, J.; Guy, R. H. *Adv. Drug Delivery Rev.* **2004**, *56*, 619.
(2) Isaksson, J.; Kjäll, P.; Nilsson, D.; Robinson, N.; Berggren, M.; Richter-Dahlfors, A. *Nat. Mater.* **2007**, *6*, 673.
(3) Sze, S. *Semiconductor devices: Physics and technology*, 2nd ed.; John Wiley & Sons: New York, 2002.
(4) Karnik, R.; Fan, R.; Yue, M.; Li, D. Y.; Yang, P. D.; Majumdar, A. *Nano Lett.* **2005**, *5*, 943.
(5) Nam, S. W.; Rooks, M. J.; Kim, K. B.; Rossnagel, S. M. *Nano Lett.* **2009**, *9*, 2044.
(6) Cheng, L. J.; Guo, L. J. *ACS Nano* **2009**, *3*, 575.
(7) Kim, K. B.; Han, J. H.; Kim, H. C.; Chung, T. D. *Appl. Phys. Lett.* **2010**, 96.
(8) Kontturi, K.; Murtomäki, L.; Manzanares, J. A. *Ionic transport processes: In electrochemistry and membrane science*; Oxford University Press: Oxford, U.K., 2008.
(9) Strathmann, H.; Krol, J. J.; Rapp, H. J.; Eigenberger, G. *J. Membr. Sci.* **1997**, *125*, 123.
(10) Mafe, S.; Ramirez, P. *Acta Polym.* **1997**, *48*, 234.
(11) Xu, T. W. *J. Membr. Sci.* **2005**, *263*, 1.
(12) Han, J. H.; Kim, K. B.; Kim, H. C.; Chung, T. D. *Angew. Chem., Int. Ed.* **2009**, *48*, 3830.
(13) Tybrandt, K.; Larsson, K. C.; Richter-Dahlfors, A.; Berggren, M. *Proc. Natl. Acad. Sci. U. S. A.* **2010**, *107*, 9929.
(14) *High Speed Heterostructure Devices*;Beer, A. C., Weber, E. R., Willardson, R. K., Kiehl, R. A., Sollner, T. C. L. G., Eds.; Academic Press: San Diego, 1994; Vol. 41.
(15) Chiang, C. K.; Fincher, C. R.; Park, Y. W.; Heeger, A. J.; Shirakawa, H.; Louis, E. J.; Gau, S. C.; Macdiarmid, A. G. *Phys. Rev. Lett.* **1977**, *39*, 1098.
(16) Roncali, J. *Chem. Rev.* **1992**, *92*, 711.
(17) Heywang, G.; Jonas, F. *Adv. Mater.* **1992**, *4*, 116.
(18) Tehrani, P.; Robinson, N. D.; Kugler, T.; Remonen, T.; Hennerdal, L.-O.; Hall, J.; Malmstrom, A.; Leenders, L.; Berggren, M. *Smart Mater. Struct.* **2005**, *14*, 21.
(19) Pei, Q.; Zuccarello, G.; Ahlskog, M.; Inganäs, O. *Polymer* **1994**, *35*, 1347.
(20) Manzanares, J. A.; Murphy, W. D.; Mafe, S.; Reiss, H. *J. Phys. Chem.* **1993**, *97*, 8524.
(21) Zabolotskii, V. I.; Manzanares, J. A.; Mafe, S.; Nikonenko, V. V.; Lebedev, K. A. *Russ. J. Electrochem.* **2002**, *38*, 819.
(22) Sokirko, A. V.; Ramirez, P.; Manzanares, J. A.; Mafe, S. *Ber. Bunsen-Ges.* **1993**, *97*, 1040.
(23) Simon, D. T.; Kurup, S.; Larsson, K. C.; Hori, R.; Tybrandt, K.; Goiny, M.; Jager, E. H.; Berggren, M.; Canlon, B.; Richter-Dahlfors, A. *Nat. Mater.* **2009**, *8*, 742.
(24) Tybrandt, K.; Larsson, K. C.; Kurup, S.; Simon, D. T.; Kjäll, P.; Isaksson, J.; Sandberg, M.; Jager, E. W. H.; Richter-Dahlfors, A.; Berggren, M. *Adv. Mater.* **2009**, *21*, 4442.
(25) Mabeck, J. T.; Malliaras, G. G. *Anal. Bioanal. Chem.* **2006**, *384*, 343.
(26) Weigl, B. H.; Bardell, R. L.; Cabrera, C. R. *Adv. Drug Delivery Rev.* **2003**, *55*, 349.
(27) Abidian, M. R.; Kim, D. H.; Martin, D. C. *Adv. Mater.* **2006**, *18*, 405.
(28) Bernards, D. A.; Malliaras, G. G. *Adv. Funct. Mater.* **2007**, *17*, 3538.